Reconstructed membrane vesicles from the microalga Dunaliella as a potential drug delivery system

Maja Levak Zorinc, Irem Demir-Yilmaz, Cécile Formosa-Dague, Ivna Vrana, Blaženka Gašparović, Lucija Horvat, Ana Butorac, Ruža Frkanec, Nadica Ivošević Denardis

Bioelectrochemistry 150 (2023) 108360

Contents lists available at ScienceDirect

Bioelectrochemistry

journal homepage: www.journals.elsevier.com/bioelectrochemistry

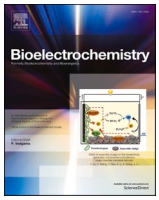

Reconstructed membrane vesicles from the microalga *Dunaliella* as a potential drug delivery system

Maja Levak Zorinc [a], Irem Demir-Yilmaz [b,c], Cecile Formosa-Dague [b], Ivna Vrana [a], Blaženka Gašparović [a], Lucija Horvat [a], Ana Butorac [d], Ruža Frkanec [e], Nadica Ivošević DeNardis [a,*]

[a] *Ruđer Bošković Institute, Zagreb, Croatia*
[b] *TBI, Université de Toulouse, INSA, INRAE, CNRS, Toulouse, France*
[c] *LAAS, Université de Toulouse, CNRS, Toulouse, France*
[d] *Biocentre Ltd., Zagreb, Croatia*
[e] *Centre for Research and Knowledge Transfer in Biotechnology, University of Zagreb, Croatia*

ARTICLE INFO

Keywords:
Drug delivery
Membrane vesicle
Microalgae
Nanomechanics
Permeability

ABSTRACT

The aim of this biophysical study is to characterize reconstructed membrane vesicles obtained from microalgae in terms of their morphology, properties, composition, and ability to transport a model drug. The reconstructed vesicles were either emptied or non-emptied and exhibited a non-uniform distribution of spherical surface structures that could be associated with surface coat proteins, while in between there were pore-like structures of up to 10 nm that could contribute to permeability. The reconstructed vesicles were very soft and hydrophilic, which could be attributed to their composition. The vesicles were rich in proteins and were mostly derived from the cytoplasm and chloroplasts. We demonstrated that all lipid classes of *D. tertiolecta* are involved in the formation of the reconstructed membrane vesicles, where they play fundamental role to maintain the vesicle structure. The vesicles appeared to be permeable to calcein, impermeable to FITC-ovalbumin, and semipermeable to FITC-concanavalin A, which may be due to a specific surface interaction with glucose/mannose units that could serve as a basis for the development of drug carriers. Finally, the reconstructed membrane vesicles could pave a new way as sustainable and environmentally friendly marine bioinspired carriers and serve for studies on microtransport of materials and membrane-related processes contributing to advances in life sciences and biotechnology.

1. Introduction

The development of drug delivery systems has been extensively researched [1–4]. Traditionally, lipid-based drug delivery systems have been the most prominent, followed by inorganic and polymer-based drug delivery systems [5–8]. Since none of these delivery systems mimic the complexity of natural biological membranes, interest in cellular or cell-derived counterparts using human (red blood cells, stem cells, immune cells), animal, and plant cells has increased dramatically over the past decade [4,9–14]. Although these cells have great advantages as drug carriers, mainly because of the recognition of the cells by the target tissue, there are some disadvantages related to the survival, migration and function of the carrier cells that limit the exposure to the drug [15,16]. In addition, there is a risk of tumorigenicity, especially in stem cells [10]. Because of these problems, cell-derived drug delivery systems such as extracellular vesicles and cell membrane- coated particles are now being investigated. Extracellular vesicles are typically released physiologically or when most types of eukaryotic and some prokaryotic cells are exposed to stress [17,18]. Although there are several types of extracellular vesicles (apoptotic bodies, microvesicles, and exosomes), the focus here is on exosomes-vesicles with a diameter of 100–200 nm that can be isolated from the cell type to be treated with a drug. Because of their good biocompatibility with target tissues, many human-derived exosomal therapies are currently under investigation [4], but the cost of obtaining highly concentrated fractions is high [19]. In the last decade, the development of drug delivery systems based on microalgae has attracted considerable interest [19–22]. For example, diatoms and their biosilicified envelope can be engineered to carry

* Corresponding author.
E-mail address: ivosevic@irb.hr (N. Ivošević DeNardis).

https://doi.org/10.1016/j.bioelechem.2022.108360
Received 30 June 2022; Received in revised form 3 December 2022; Accepted 24 December 2022
Available online 27 December 2022

genes, and nucleic acids [20,23] and can also be functionalized to deliver drugs to cancer cells [9]. In addition, various types of green microalgae have been used as a source of algal exosomes (nanoalgosomes) which are also a promising type of carrier, but the disadvantage at present is also the low yield of this type of vesicle [21,22]. In particular, the green microalga *Dunaliella tertiolecta*, known as a naked cell surrounded by a thin elastic plasma membrane and a glycocalyx surface layer [40], has the potential to be used for the preparation of reconstructed membrane vesicles. Recently, a new type of autofluorescent reconstructed vesicles has been reported, which are not extracellular vesicles and have a different formation mechanism [24]. Due to the hypoosmotic shock of soft cells, cells burst, intracellular material is released, and the remaining membrane fragments self-assemble due to various non-covalent interactions, spontaneously forming reconstructed membrane vesicles. The aim of this study is to characterize the reconstructed membrane vesicles in terms of their morphology, properties, and composition as well as their ability to transport selected fluorescent dyes. Such reconstructed membrane vesicles could serve as a basis for the development of marine bioinspired carriers for advanced biotechnological applications.

2. Materials and methods

2.1. Cell suspensions

The unicellular marine alga *Dunaliella tertiolecta* Butcher (Chlorophyceae, CCMP 1320, Culture Collection Bigelow Laboratory for Ocean Sciences, Bigelow, MN, USA, length: 6–12 μm) was grown in natural seawater. Natural seawater was collected from a depth of 25 m (Stončica Bay, Vis Island, the Adriatic Sea) during fieldwork on November 21, 2019 and used for cell culture. The seawater was stored in the dark in a cold room at +4 °C. Before use, the seawater was filtered through a Milipore filter with a pore size of 0.2 μm to remove living and non-living particles. The salinity of the seawater was determined with a hand refractometer and was 38, which means 38 g of salts per liter of water. Nowadays, the salinity is given without a unit, because it is expressed as the ratio of the electrical conductivity of the seawater sample to the electrical conductivity of the potassium chloride standard solution at 15 °C and a pressure of 1 atmosphere. In addition, the seawater was enriched with components of the F-2 medium [25]. After adding appropriate aliquots of $NaNO_3$ and trace metals, the solution was sterilized in a microwave oven (medium high) for 3 min and held under a UV lamp for 7 min. After the medium cooled to room temperature in a sterile chamber, aliquots of NaH_2PO_4 and vitamins were previously filtered through an acrodisc with a pore diameter of 0.20 μm. Under sterile conditions, an aliquot of cells is added so that the initial number of monoculture corresponds to approximately 4×10^4 cells mL^{-1}. The flasks were sealed with sterile cotton plugs to prevent contamination. Cells were cultured under ambient conditions (25 °C, 12 h light:12 h dark, shaking (20 rpm)). The average cell number in triplicate samples was determined using a Fuchs-Rosenthal haemocytometer (Fein-Optik Jena, Germany, depth 0.2 mm) and a light microscope (Olympus BX51, Olympus Corporation, Japan) at 400 × magnification. The cell density was 6×10^6 cells/mL after 10 days of growth. Cells were separated from the growth medium by gentle centrifugation (1500 × *g*, 5 min). The loose pellet was washed several times with filtered seawater by centrifugation and used to prepare vesicles.

2.2. Preparation of the reconstructed membrane vesicles

The reconstructed membrane vesicles, called ghost vesicles, were produced by osmotic shock of the photosynthetic marine microalga *Dunaliella tertiolecta* in early stationary phase. The diagram with the protocol for vesicle preparation can be found in the supplementary material as Fig. S1. The loose algal cell pellet was isolated from 500 mL of cell growth medium by gentle centrifugation (1500 × *g* for 5 min) and rinsed three times with filtered seawater (0.22 μm) to remove metabolites, other extracellular material, and particles. The final supernatant was completely removed and 4 mL of the loose algal cell pellet was diluted 40 times with ultrapure water, shaken vigorously, and then allowed to stand at room temperature for 30 min. During this time, osmotic shock of the cells was allowed to occur. The cells disintegrated and formed a mixture of spontaneously assembled vesicles with and without attached cellular material and clumps of free-flowing debris. Further purification steps were performed to obtain the cleanest possible suspension of empty ghost vesicles.

In the next step, samples were centrifuged at 1500 × *g* for 4 min. The resulting pellets and supernatants were examined under a light microscope. Pellet 1 contained a large amount of released intracellular material, nonempty vesicles, and empty vesicles. Supernatant 1, which contained empty vesicles, vesicles with some adherent material, and a small amount of free debris, was centrifuged at 10 000 × *g* for 10 min at 10 °C. The resulting pellet 3 contains mainly debris and some vesicles, while supernatant 3 contains mainly empty reconstituted vesicles and vesicles with some adherent material concentrated in a thin viscous layer near the pellet 3. The fraction of concentrated vesicles from supernatant 3 is stabilized with Tris-HCl buffer and $MgCl_2$ (both final concentrations were 10 mM, pH 8.0). The concentration of reconstructed membrane vesicles in the suspension generally ranges from 10^4 to 10^6 vesicles/mL and is up to 30 μm in size.

2.3. Epifluorescence and confocal laser scanning microscopy

An Olympus BX 51 fluorescence microscope was used for preparation of reconstructed vesicles and determination of cell and vesicle density. Confocal measurements were performed with a Leica TCS SP8 laser scanning confocal microscope equipped with a white light laser and a 63× (N.A. = 1.4) oil immersion objective. The excitation and emission spectra generated by the microscope were used to optimize the emission windows.

Lipophilic membrane stain DiI (Sigma, excitation maximum 552 nm, detection range 570–600 nm) was used to improve visualization of the vesicles. A stock solution of DiI at a concentration of 200 μM was prepared in anhydrous DMSO. Calcein, FITC-concanavalin A, and FITC-ovalbumin were used to test transportability of the vesicles. Calcein (Sigma, excitation maximum 488 nm, detection range 500–540 nm) was prepared as a stock solution (20 mM in ultrapure water). FITC-concanavalin A (Sigma) and FITC-ovalbumin (Invitrogen, Life technologies, USA; excitation maximum 488 nm, detection range 500–540 nm) were prepared in ultrapure water at a concentration of 1 mg/mL. FITC-dextrans with different molecular weights (Sigma, 3–5 kDa, 10 kDa, 20 kDa, and 70 kDa) were used for permeability assay. All FITC-dextrans were prepared in ultrapure water at 1 mg/mL.

SPY555-tubulin (Tebu-bio SAS, excitation maximum 555 nm, detection range 570–620 nm) was used as a probe for imaging of microtubules. The content of the SPY probe tube was prepared in 50 μL DMSO solution and diluted 100-fold before imaging. Autofluorescence of the reconstructed membrane vesicles was also recorded (excitation 555 nm, detection range 660–720 nm).

2.4. Sample preparation for confocal imaging

Before use, the slides were washed with ethanol and rinsed several times with water. After drying with a stream of nitrogen, 50 μL of polyethylenimine (PEI, 0.2% w/v) was added to the slide for 30 min. The PEI droplet was then removed and rinsed three times with ultrapure water. Finally, 20 μL of an aliquot of the vesicles was added to the modified slide and allowed to stand for 30 min. Prior to imaging, the fluorescent dye DiI was added at a final concentration of 2 μM, followed by the addition of FITC-dextran or selected fluorescent dyes. Calcein was added at a final concentration of 5 μM. FITC-concanavalin A, FITC-ovalalbumin and FITC-dextran were added to the sample in aliquots

between 1 and 4 μL, to achieve final concentrations between 50 and 200 μg/mL.

2.4.1. Analysis of vesicle permeability with image J software

Fluorescence intensity analysis for vesicle permeability study was performed using Image J (software version 1.53 k, National Institute of Healh, USA). The measured fluorescence intensities inside the vesicles were compared with the fluorescence intensity outside the vesicles on the confocal images. For each dextran molecular weight, at least 50 vesicles were analyzed on an 8 × 8 μm image and, in parallel, the vesicle population was analyzed on 25 × 25 μm images. Measurements were always performed on clear background segments and at a distance of at least 20% from the membrane to exclude possible interference with membrane luminescence. The relative fluorescence intensity within the vesicles was expressed as a percentage of the fluorescence intensity of the background.

2.5. Sample preparation for AFM measurements

For AFM imaging in air, a volume of 5 μL of the suspension containing the reconstructed membrane vesicles was pipetted directly onto freshly cleaved mica and dried in a closed Petri dish for 1 h before imaging. AFM imaging of the vesicles was performed using a MultiMode Scanning Probe Microscope with Nanoscope IIIa controller (Bruker, Billerica USA) and a 125 μm Vertical Engagement (JV) scanner. Images were acquired in contact mode using a standard silicon nitride tip (DNP-10, Bruker, nominal frequency 18 kHz, nominal spring constant of 0.06 N/m) with a scan resolution of 512 samples per line. Sampling rates were typically optimized to 1–2 Hz. Images were processed and analyzed using NanoScopeTM software (Digital Instruments, version V614r1). The force was kept at the lowest possible value to minimize interaction forces between the tip and the surface. Measurements were performed in air, at room temperature and 50–60 % relative humidity, so that the samples have a small hydration layer that helps to preserve the structure [26]. All images are presented as raw data, except for the two-dimensional first-order flattening.

For AFM imaging in liquid, vesicles were first immobilized on glass slides coated with PEI. For this purpose, freshly activated slides were coated with a 0.2% PEI solution in deionized water and incubated overnight. The slides were then rinsed with deionized water and dried with nitrogen. A total of 1 mL of the vesicle suspension was then applied to the PEI-coated slide, allowed to stand for 30 min, and rinsed with Tris-HCl buffer and $MgCl_2$ (both final concentrations were 10 mM, pH 8.0) to remove nonsticky vesicles. Height images of the reconstructed membrane vesicles were acquired with the quantitative imaging (QI) mode of Nanowizard III AFM (Bruker, USA) using MSCT cantilevers (Bruker, nominal spring constant of 0.01 N/m), in 10 mM Tris-HCL with addition of 10 mM $MgCl_2$ buffer. Images were acquired at a resolution of 150 × 150 pixels, applying a force of <1 nN. In all cases, the spring constants of the cantilevers were determined using the thermal noise method prior to imaging [27]. The obtained height images were then analyzed using Data Processing Software (Bruker, USA).

2.6. AFM force spectroscopy

AFM in force spectroscopy mode was used to measure the nanomechanical properties of vesicles. A maximum force of 0.5 nN was applied using MSCT cantilevers (Bruker, nominal spring constant of 0.1 N/m). In each case, 18 reconstructed vesicles immobilized on PEI-coated glass slides were analyzed from 2 independent series (400 force curves were recorded for each algal vesicle). Young's moduli were then calculated from the 300-nm indentation curves using the Hertz model [28], in which the force F, indentation (δ), and Young's modulus (Ym) follow equation (1), where α is the tip aperture angle (17.5°) and υ is the Poisson's ratio (arbitrarily assumed to be 0.5). The spring constants of the cantilevers were determined before each experiment using the thermal noise method [27].

$$F = \frac{2 \times Ym \times \tan\alpha}{\pi \times (1 - \upsilon^2) \times \delta^2} \quad (1)$$

For the hydrophobicity experiments, AFM was used in combination with FluidFM as described in [29]. Briefly, an air bubble was generated using a Nanowizard III AFM (Bruker, USA) equipped with FluidFM technology (Cytosurge AG, Switzerland). Experiments were performed in PBS at pH 7.4 using microfluidic micropipette probes with an aperture of 8 μm (spring constant of 0.3 N/m, Cytosurge AG, Switzerland). The probes were calibrated using the thermal noise method [27] before the measurements. Then, the interactions between the bubbles formed at the aperture of the microfluidic micropipette probes and 7 algal vesicles were measured in force spectroscopy mode with a constant applied force of 0.5 nN. Force curves (400 force curves for each vesicle) were recorded with a retraction z-length of up to 2 μm and a constant retraction speed of 1.0–2.0 μm/s. The adhesion force between the bubble and the algal vesicle was calculated by measuring the height of the adhesion peak using Bruker data processing software (Bruker, USA).

2.7. Lipid extraction and analysis

Lipid extractions were performed from 50 mL of an algal cell monoculture in the early stationary growth phase and 15 mL of an algal-derived vesicle suspension. Samples were filtered through a pre-combusted (450 °C/5h) 0.7 μm Whatman GF/F filters. Extraction was performed using a modified one-phase solvent mixture of dichloromethane-methanol–water [30]: 10 mL of one-phase solvent mixture dichloromethane/methanol/deionized water (1:2:0.8 v/v/v) and 5 μg of standard methyl stearate (to estimate recoveries in subsequent steps of sample analysis) were added to the cut filters. They were then ultrasonicated for 3 min, stored overnight in the refrigerator, filtered through a sinter funnel into a separatory funnel, washed again with 10 mL of the one-phase solvent mixture and then washed once with 10 mL of dichloromethane/0.73% NaCl solution (1:1 v/v) and finally with 10 mL of dichloromethane. Lipid extracts collected in dichloromethane were evaporated to dryness under nitrogen flow and dissolved in 34–54 μL dichloromethane before analysis. All solvents were purchased from Merck Corporation (USA).

Lipid classes were determined by thin-layer chromatography with flame ionization detection (TLC-FID; Iatroscan MK-VI, Iatron, Japan). Lipids were separated on Chromarods SIII. Quantification was determined by external calibration of lipid classes. Analysis was performed using a hydrogen flow of 160 mL/min and an airflow of 2000 mL/min. We determined representative membrane lipid classes: three glycolipids (monogalactosyldiacylglycerols (MGDG), digalactosyldiacylglycerols (DGDG), and sulfoquinovosyldiacylglycerols (SQDG)), three phospholipids (phosphatidylglycerols (PG), phosphatidylethanolamines (PE), and phosphatidylcholines (PC)) and sterols (ST), and lipid degradation indices (DI) which include free fatty acids, fatty alcohols, 1,3-diacylglycerols, 1,2-diacylglycerols and monoacylglycerols. The total lipid concentration is the sum of the individual lipid classes. The standard deviation determined from duplicate runs was 0–15%. The detailed procedure is described in [31,32].

2.8. Protein analysis

The concentration of total proteins was determined by the Bradford method [33] in duplicate samples. For protein analysis, 200 μL of the vesicle sample was mixed with 20 μL 10% SDS (pH = 7.2) and boiled in a water bath for 1 min; 5 volumes of ice-cold acetone were added to the sample, and the proteins were precipitated overnight at −20 °C. The precipitated proteins were pelleted by centrifugation (10 000 × *g*, 4 °C, 10 min). The pellet was dissolved in 25 μL 25 mM ammonium bicarbonate buffer (pH = 7.8). Digestion was performed with trypsin (Promega, SAD) overnight at 37 °C. The peptides obtained after

digestion were separated according to the method described in [34]. NanoLC system Dionex Ultimate 3000 RSLCnano (Thermo Fisher Scientific, Germany) coupled to Proteineer fcII (Bruker, Germany) was used for separation and peptide collection. Mass spectrometry (MS) was performed using an Autoflex speed MALDI-TOF /TOF analyzer (Bruker, Germany). Mass spectra were obtained according to the method described in [34]. Protein identification was performed using ProteinScape software version 3.0 (Bruker, Germany) with the search engine MASCOT. An in-house database of protein sequence data of *D. tertiolecta* was used. Protein sequence data were downloaded from the UniProt database (accessed March 19, 2022, no. of entry 12 786). Search parameters were set as follows: a missing trypsin cleavage, oxidation on methionine as a variable modification, precursor ion mass tolerance 50 ppm, and fragment ion mass tolerance 0.6 Da. The protein–protein interaction network (PPI) of the identified proteins was generated using STRING version 11.0 with a minimum confidence level of 0.4. A multiple sequence search was used.

2.9. Carbohydrate analysis

The standard stock solution of glucose (1 mg/mL) was diluted to a concentration of 0–0.1 mg/mL and used to construct the calibration curve. The anthrone reagent was prepared as follows: 200 mg of anthrone (ACS reagents, Sigma-Aldrich) was added to a 100 mL volumetric flask, and the volume was adjusted to 100 mL with 96% sulfuric acid (Biochem). The vesicle suspension sample was diluted 1:10 with deionized water. 1 mL of the diluted glucose standards or sample was added to the tube along with 4 mL of anthrone reagent, vortexed, and incubated at 80 °C in a water bath (Lauda, Alpha RA8) for 10 min. After cooling on ice to room temperature, absorbance was determined at 630 nm in duplicate samples (UV/VIS spectrophotometer, Cary 100, Agilent Technologies). Total carbohydrate content is expressed as glucose equivalent in mg per mL of sample.

3. Results

3.1. Nanomorphological characterization of the reconstructed membrane vesicles

Fig. 1 shows reconstructed membrane vesicles deposited on mica and imaged by AFM in air.

The topographic image shows densely packed vesicles, many of which overlapped on the outside (Fig. 1a). The vesicles were nearly round, although some elongation may have been due to the drying step and less than optimal adhesion to the mica surface. Cross-sectional analysis of 21 vesicles shows that the diameter and height of the vesicles were 13.5 ± 2.1 μm and 87.9 ± 6.8 nm, respectively. Thus, the vesicles were not deflated but contained a thick membrane and some embedded intracellular material. Topographic and 3-D views show round reconstructed membrane vesicles (Fig. 1d, 1f). Cross-sectional analysis shows that the diameter and height of the vesicle were 10.2 μm and 62.8 nm, respectively, indicating embedded intracellular material and particles adhering to the membrane surface (Fig. 1e). Topographic and 3-D views show individual reconstructed membrane vesicle that can be considered nearly depleted (Fig. 1g, 1i). Cross-sectional analysis shows that the diameter and height of the vesicle were 3.0 μm and 20.2 nm, respectively, while the internal height of the vesicle was between 2 and 4 nm. Insights into the surface structure of the reconstructed membrane obtained from the AFM deflection image and 3D view are provided in Fig. S2. The heterogeneously distributed spherical surface structures were predominantly about 100 nm in diameter and 5–10 nm in height, with pits in between. The roughness of the vesicles in air was determined on the areas of 8 × 8 μm on the surface of 21 vesicles and corresponded to 11.5 ± 1.4 nm. The reconstructed membrane vesicles were also imaged by AFM in liquid. The height image and the corresponding 3D view of a vesicle are shown in Fig. 2a and 2b, respectively.

The cross-section (Fig. 2c), taken along the white line in Fig. 2b, shows the morphology of the surface. The reconstructed membrane vesicle had a round shape with a height of more than 2 μm. The average maximum height of the vesicles measured on 6 different vesicles was 2.92 ± 0.50 μm, which was much higher than under near-dry conditions. This difference is probably due to the hydration of the vesicles, which increases their size. Finally, the roughness of the vesicles was also measured under liquid conditions. For this purpose, high-resolution images were taken on areas of 1.5 × 1.5 μm on the surface of six vesicles. An example of such an image is shown in Fig. 2d and 2e along with the cross-section. The average roughness found was 9.29 ± 5.36 nm. The large standard deviation in this case illustrates the heterogeneity of the vesicle surfaces.

3.2. Determination of pore size on reconstructed membrane vesicles

Fig. 3 shows representative confocal images of Dil-stained reconstructed membrane vesicles after addition of FITC-dextran with selected molecular weights of 3–5 kDa, 10 kDa, 20 kDa, and 70 kDa.

The fluorescence intensity inside and outside the vesicle was completely balanced, i.e., the relative fluorescence intensity inside the vesicle is 95% of the fluorescence intensity outside the vesicle. Therefore, the vesicles were assumed to be fully permeable to 3–5 kDa dextran (Fig. 3a). After addition of 10 kDa FITC-dextran, the fluorescence intensity inside the vesicles was 84% of the background fluorescence intensity, so the reconstructed membrane vesicles were also predominantly permeable to 10 kDa dextran (Fig. 3b). Fig. 3c shows reconstructed membrane vesicles in contact with 20 kDa FITC-dextran. Quantitative analysis shows that the fluorescence intensity inside the vesicles decreased to 37% of the background fluorescence intensity. Thus, the reconstructed membrane vesicles were predominantly impermeable to dextran of this size. Finally, after the addition of 70 kDa dextran, the highest fluorescence intensity was outside the vesicles, indicating that the majority of the reconstructed membrane vesicles were predominantly impermeable to dextran of this molecular weight (Fig. 3d). The fluorescence intensity within the vesicles in contact with 70 kDa dextran was 17% of the background fluorescence intensity. Overall, the permeability of reconstructed membrane vesicles decreased with an increase in the molecular weight of dextran from 3 to 70 kDa (Fig. 4). Between 10 and 20 kDa, a significant decrease in the accumulation of dextran in the vesicles was observed. A large standard deviation illustrates the heterogeneity of the pores on the membrane surface. Therefore, 20 kDa can be considered as a threshold value.

3.3. Nanomechanical and chemical characterization of the reconstructed membrane vesicles

Nanoindentation experiments were performed to obtain quantitative information on the nanomechanical properties of the reconstructed vesicles in terms of Young's modulus (Ym) (Fig. 5a and 5b).

In these experiments, a cantilever with known mechanical properties was pressed against the vesicle surface with a certain force. In this way, the Ym value of the sample can be determined, a parameter that reflects its resistance to compression. Thus, Ym is a value related to the rigidity; the higher the Ym value, the more rigid the sample. In this study, nanoindentation measurements were performed on areas of 1.5 × 1.5 μm on the surface of 17 reconstructed membrane vesicles obtained from two independent batches of samples. Nanoindentation measurements provide access to force–displacement curves. From these curves, Ym values were determined by converting the force curves into force versus indentation curves (black line in the inset of Fig. 5a) and then fitting with the Hertz model [28] (orange line in Fig. 5a). Quantitative analysis of all Ym values extracted from the force curves yielded an average Ym value of 0.37 ± 0.31 kPa (n = 5959 force curves).

The hydrophobic properties of the reconstructed membrane vesicles

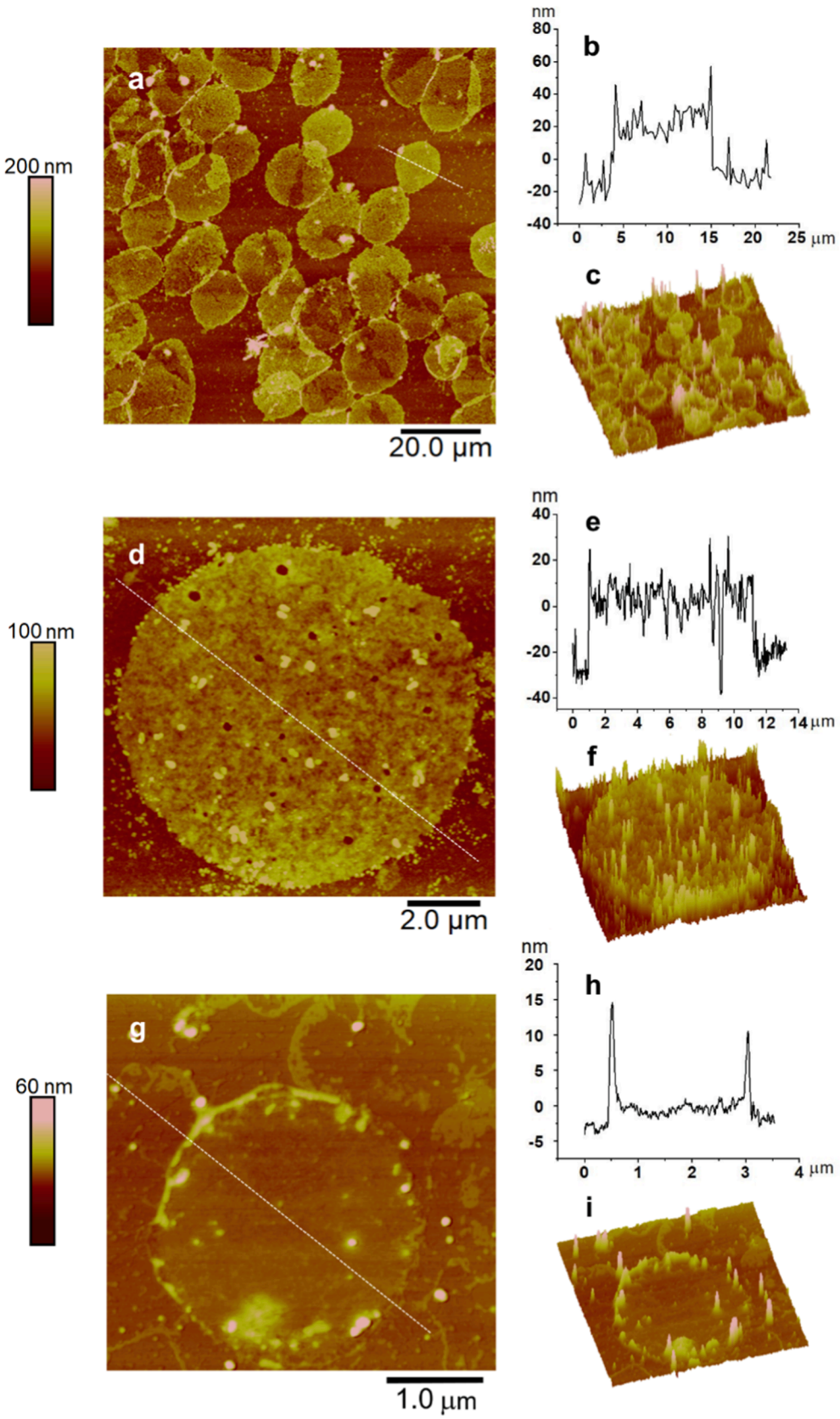

Fig. 1. AFM images of densely packed reconstructed membrane vesicles (a), individual vesicle with embedded material (d), and individual reconstructed nearly empty membrane vesicle (g) with corresponding cross-sections along the indicated lines (b, e, h) and 3D views (c, f, i), respectively. Scan sizes are 100 × 100 μm (a), 11 × 11 μm (d), 4 × 4 μm (g).

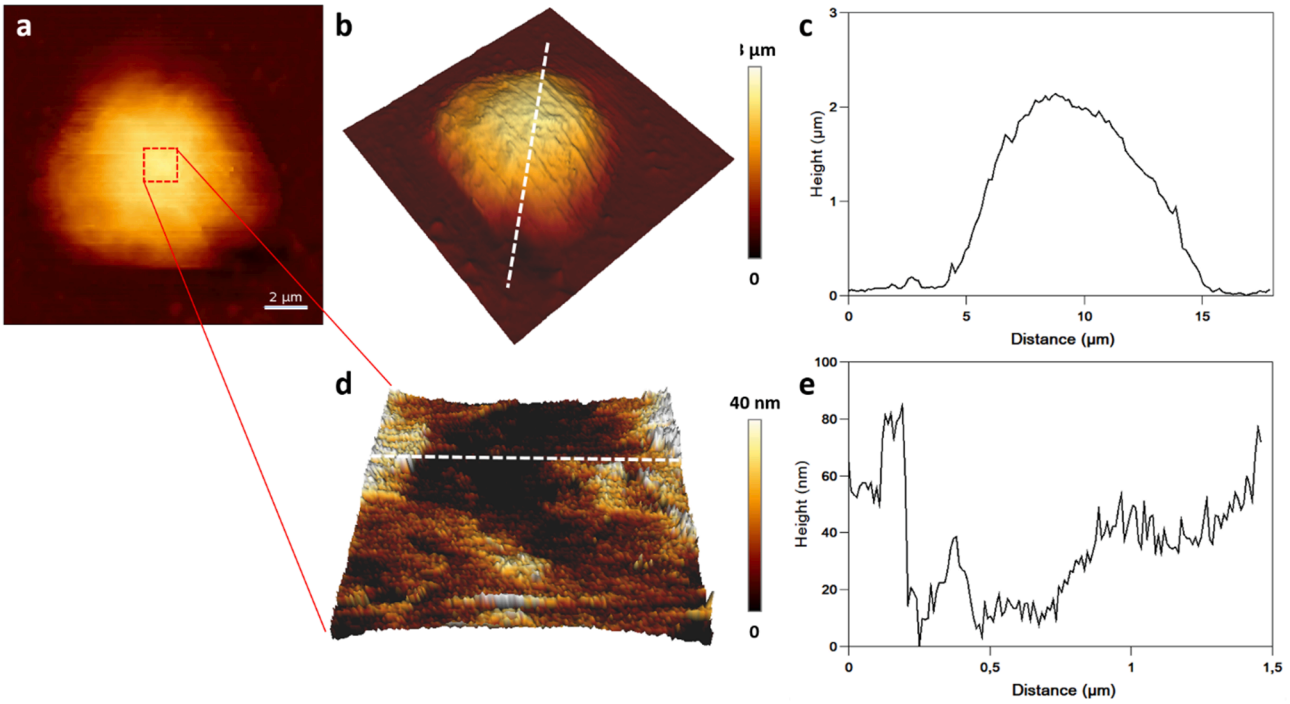

Fig. 2. AFM height image of a reconstructed membrane vesicle recorded in liquid (a) and the corresponding 3D view (b). Cross-sectional data (c) acquired along the white line in (b). High-resolution height image (d) taken in the area indicated by the red square in (a), and cross-sectional data (e) taken along the white line in (d).

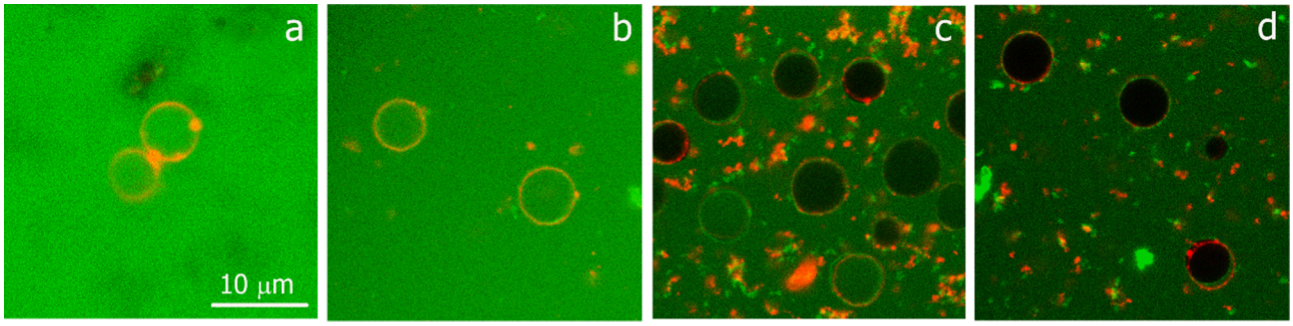

Fig. 3. Representative confocal images of DiL stained reconstructed membrane vesicles after addition of FITC-dextrans with different molecular weights: 3–5 kDa, 10 kDa (a), 20 kDa (b), and 70 kDa (c). Panel a shows vesicles where the fluorescence inside and outside the vesicle was the same, indicating that the corresponding vesicles are permeable to dextran FITC 3–5 kDa. Panel b shows vesicles that were mainly permeable to dextran FITC 10 kDa. Panel c shows the larger population of vesicles with little or no fluorescence within the vesicle, which would correspond to the semipermeable and impermeable vesicle fractions, whereas the fraction of permeable vesicles was smaller. Panel d shows the population of vesicles that were predominantly impermeable to dextran FITC 70 kDa.

were also determined. For this purpose, we used a recently developed method consisting in studying the interactions between samples and air bubbles prepared with FluidFM technology [29], which combines AFM with microfluidics [35]. Air bubbles in water behave like hydrophobic surfaces. Therefore, if interactions between bubbles and vesicles are recorded, it means that the vesicles have hydrophobic properties. This method has been used to measure the hydrophobic properties of complex surfaces such as cells [29] or microplastic particles [36] and is a more accurate method for measuring hydrophobicity than measuring water contact angle, which can be difficult for biological samples. Moreover, compared to classical measurements using hydrophobic AFM tips, this method has the advantage of providing access to the global hydrophobic properties of the samples, since the radius of the bubble in contact with the sample was about 1.2 µm [29], which was 60 times larger than that a regular AFM tip (20 nm) [37,38]. The results of these experiments are shown in Fig. 5b. The force curves obtained in this case show no adhesion peaks on the retraction force curves (inset in Fig. 5b), which means that the reconstructed membrane vesicles do not interact with the bubbles. These results suggest that the vesicle surface is mainly hydrophilic, whereas the hydrophobic moieties are probably hidden in the vesicle membrane.

3.4. Composition of the reconstructed membrane vesicles

3.4.1. Lipids

The concentrations of total lipids in the cells of *D. tertiolecta* and the reconstructed membrane vesicles were 9265 ± 2229 µg/L and 8957 ± 563 µg/L, respectively. The difference between *D. tertiolecta* and the reconstructed membrane vesicles was that there were approximately 1.5 times more lipids in the *D. tertiolecta* mother cell than in the reconstructed membrane vesicles. The concentration of total lipids per cell of *D. tertiolecta* was 4.03 ± 0.98 pg/cell, whereas the concentration of total lipids per vesicle was 2.63 ± 0.17 pg/vesicle. The composition of lipid classes in the cells of *D. tertiolecta* and the reconstructed membrane vesicles is shown in Fig. 6a and 6b, respectively. All lipid classes detected in the cells of *D. tertiolecta* were also embedded in vesicles.

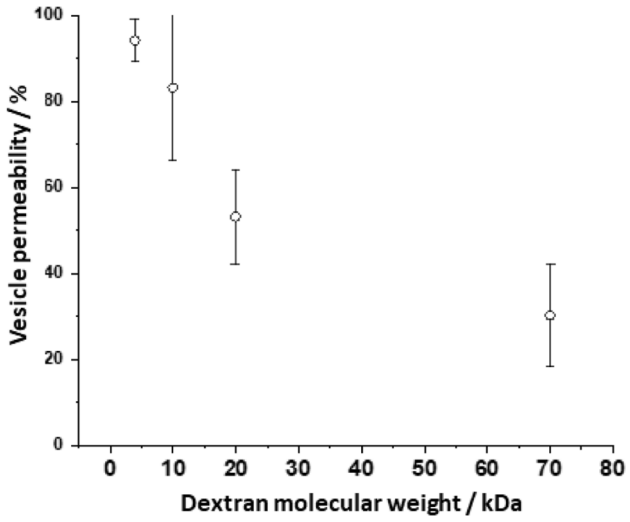

Fig. 4. Dependence of vesicle permeability on selected dextran molecular weights.

During the process of membrane reconstruction, there were no major changes in the ratios of lipid classes. Polar lipids dominated in both cells and reconstructed membrane vesicles (76.7 ± 0.5% and 80.8 ± 0.7%, respectively), with the glycolipids MGDG and the phospholipids PG being the dominant classes. MGDG contributed 30.50 ± 0.06% and 26.76 ± 0.85%, while PG contributed 16.76 ± 1.70% and 21.46 ± 0.11% in the cells of *D. tertiolecta* and reconstructed membrane vesicles, respectively.

3.4.2. Proteins

The determined concentration of total proteins in the reconstructed membrane vesicle suspension corresponded to 0.1 mg/mL. Further protein analysis was performed to identify the proteins incorporated into the vesicles. In addition, STRING analysis was used to investigate the PPI network between the identified proteins. The results are shown in Fig. 7 and Table S1. The results indicate that the proteins incorporated into the vesicles were biologically connected as a group (the calculated PPI enrichment P value was $<1.0 \times 10^{-16}$, indicating that the nodes were not random and that the observed number of edges was significant). According to the gene ontology (GO), most of the identified proteins were involved in the carbohydrate metabolic process (GO:0005975), cellular amino acid biosynthetic process (GO:0008652), photosynthesis (GO:0015979), oxidoreductase activity (GO:0016491) and microtubule-based process (GO:0007017). Judging from the

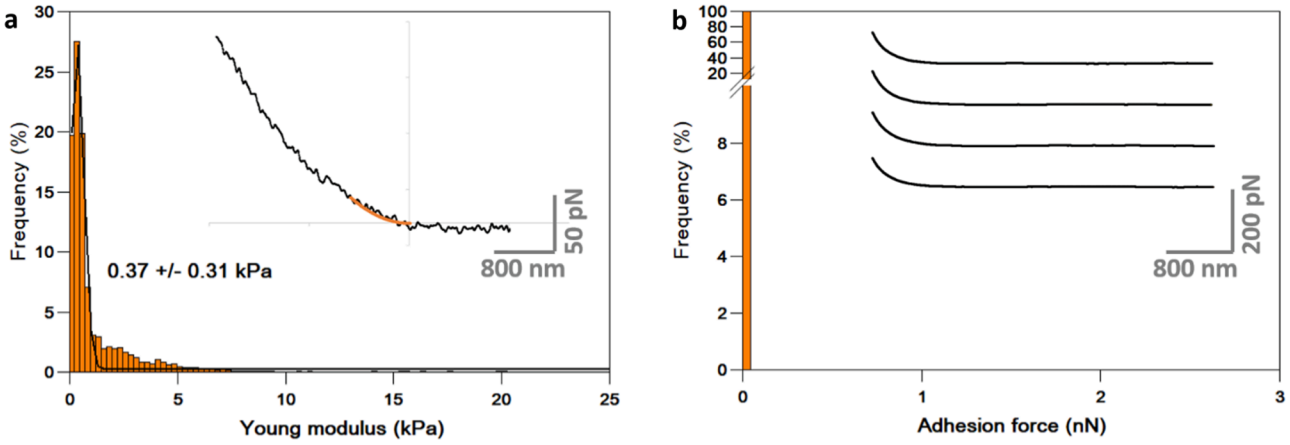

Fig. 5. The histogram shows the distribution of Young's modulus values obtained from nanoindentation measurements on areas of 1.5 × 1.5 μm on the surface of 17 cells from 2 independent batch cultures (a). The inset shows an indentation curve (black line) fitted with the Hertz model (orange line) over 300 nm indentation depth. The histogram shows the distribution of adhesion force values obtained from force spectroscopy experiments between bubbles formed with FluidFM and 7 vesicles from a batch culture (b).

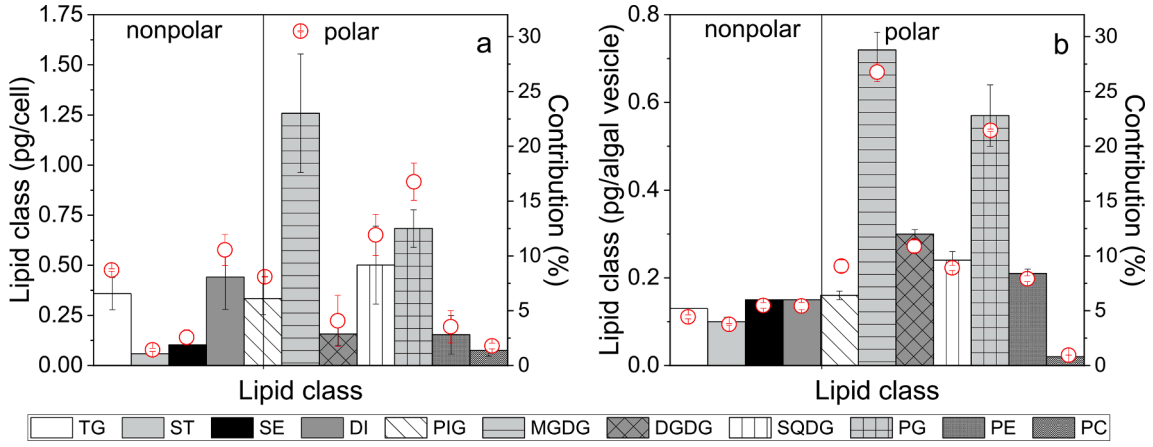

Fig. 6. Lipid class content (left y-axis, columns) and their contribution to total lipids (right y-axis, open red circles) of *D. tertiolecta* cells (a) and the reconstructed membrane vesicles (b). Data are expressed as mean ± SD.

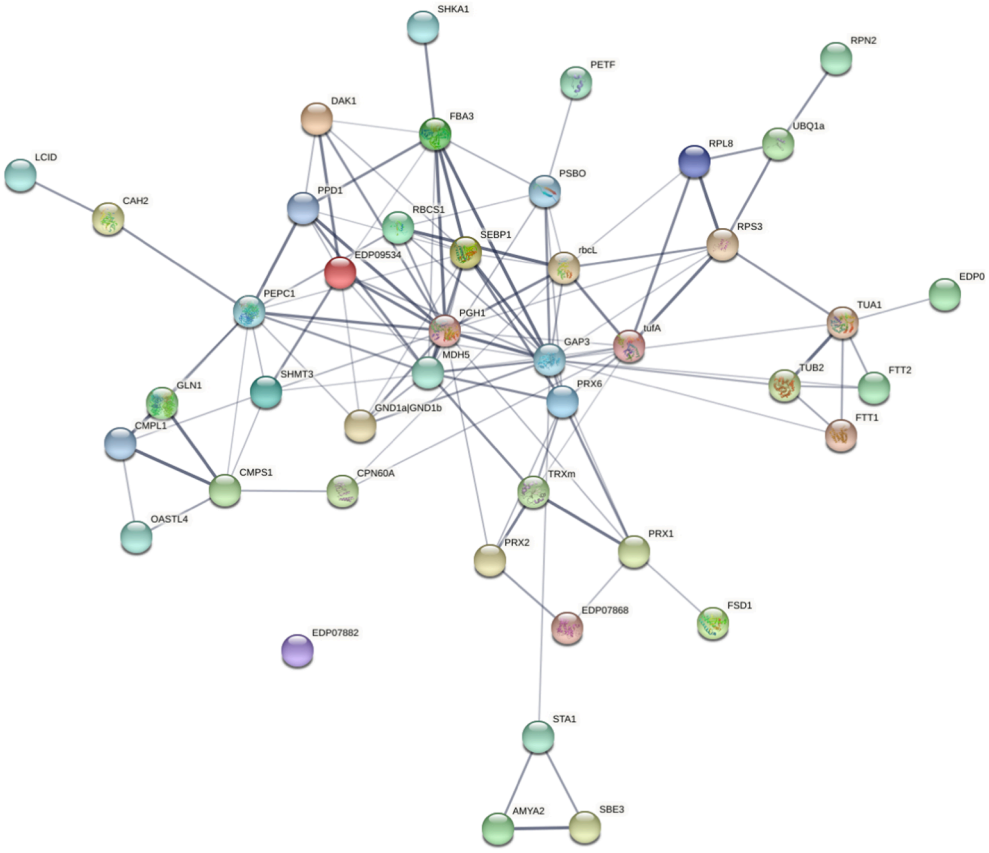

Fig. 7. Interactome shows protein–protein interactions between identified proteins in the reconstructed membrane vesicle. Colored nodes represent the proteins interrogated (Table S1), and color saturation of edges indicates the confidence of functional association.

subcellular location, most proteins originate from the cytoplasm and chloroplasts.

3.4.3. Carbohydrate content

The determined total carbohydrate concentration in the reconstructed membrane vesicle suspension corresponded to 0.087 mg/mL based on UV/VIS spectrophotometric analysis. By the HPLC-RID analysis of glucose in the sample, the glucose concentration was below the detection limit (<0.15 mg/mL).

3.5. Reconstructed membrane vesicle ability to transport model dyes

Fig. 8b shows that the fluorescence of calcein was evenly distributed inside and outside the reconstructed membrane vesicles, i.e., the vesicles behaved permeably to calcein. On the other hand, the fluorescence intensity of FITC-ovalbumin was highest outside the vesicles, whereas no fluorescence occured inside the vesicles, i.e., the vesicles were impermeable to the corresponding dye, as shown in Fig. 8e. Fig. 8h shows that the fluorescence intensity in the case of FITC-concanavalin was higher at the membrane edge than in the surrounding medium. Since the fluorescence intensity inside the vesicles was close to zero, the vesicles could either be semipermeable or a small part of the luminescence is due to the out-of-focus membrane luminescence.

4. Discussion

The major limitations in drug carrier manufacturing are protocol inefficiency, bioincompatibility and high cost. There is a great need to overcome these limitations and meet the requirements of sustainability and environmental friendliness. This can be achieved by using the microalgae presented here, which can be easily cultivated. They are widely used as a food source, dietary supplement, pharmacological agent, and energy source. On the other hand, the potential of microalgae to produce reconstructed membrane vesicles for drug transport has not been adequately explored. To address this gap, this study focuses on a comprehensive screening of reconstructed membrane vesicles by investigating the relationship between morphology, properties, and composition and testing their ability to transport a model drug to serve as an alternative carrier for advanced biotechnological applications.

We are interested in marine microalgae, in particular the widely distributed species *D. tertiolecta*, as a natural biomaterial for the preparation of reconstructed membrane vesicles based on a recently published protocol [24]. The main feature for the use of the microalga *D. tertiolecta* is that it has no cell wall, but only a glycocylyx-type cell envelope, which makes it very soft. Another advantage is its semipermeable membrane, which is why *Dunaliella* is used for osmoregulation studies. When the algae are subjected to hypoosmotic shock, the volume of the cells increases, pores form, the cells burst, intracellular material is released, and the remaining membrane fragments fuse to form reconstructed algal vesicles with high yield.

Nanomorphological characterization revealed a mixed population of micrometer-sized, nearly round, deflated and nondeflated membrane vesicles with embedded intracellular material and some adherent particles. When the vesicles are nearly deflated, the membrane thickness corresponds to 20 nm, indicating that each membrane bilayer has a thickness of 10 nm (Fig. 1h). This is consistent with the cell envelope thickness of 9 nm determined by electron microscopy [39]. This relatively high membrane thickness is likely due to the presence of water residues, other cellular components entrapped in the vesicle membrane, and the high glycoprotein content in the cell envelope. The “envelope” of *Dunaliella* cells appears to be composed of glycoproteins of 150 kDa present in the outer layer surrounding the cells [40]. AFM images (in air

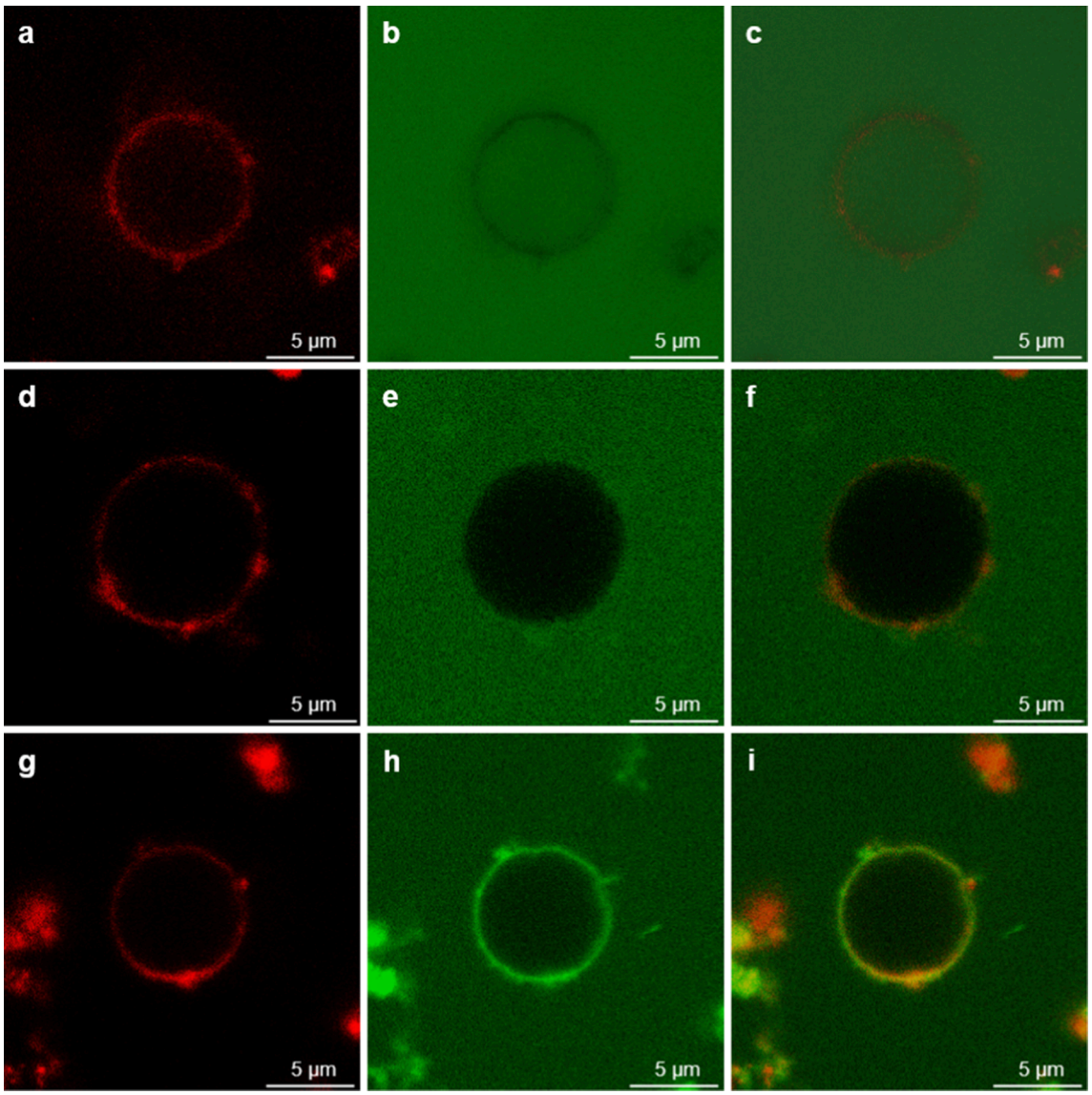

Fig. 8. Representative confocal images of reconstructed membrane vesicles stained with DiI (a,d,g), after addition of calcein (b), overlapping image (c), after addition of FITC-ovalbumin (e) and overlapping image (f), after addition of FITC-concanavalin A (h) and overlapping image (i).

and in liquid) also showed that the vesicle surface is uneven and contains irregularly distributed spherical surface structures and pits (Figs. 1, 2, S2). Based on their height, these could be surface coat proteins with different functions [41,42]. A similar surface roughness was imaged by AFM in ghosts of red blood cells [43–45]. This revealed the structure of the cytoskeleton, which consists of spectrin dimers connected by actin filaments and proteins to form a two-dimensional network [43]. Actin filaments were also observed in our system of reconstructed membrane vesicles, but only within the membrane [24]. The spherical surface structures on the reconstructed membrane vesicles are assembled in a specific way to form pore-like structures, which could be responsible for the permeability of the vesicles to hydrophilic molecules. A permeability assay with labeled dextrans of different molecular weights showed that the reconstructed membrane vesicles were predominantly impermeable to FITC-dextran of 20 kDa and above (Figs. 3, 4). The variations in permeability are related to a small fraction of vesicles with larger pores that did not close after osmotic shock and to dextran molecules, which are known to be deformable and therefore have non-uniform molecular size [46]. The hydrodynamic radius of the dextran 20 kDa corresponds to 5.2 ± 0.5 nm [47]. The pore sizes of the reconstructed membrane vesicles should be predominantly smaller than dextran of this size. Therefore, the diameter of pores in reconstructed membrane vesicles could be as small as 10 nm. In addition, pore properties (lipophilicity/hydrophilicity) may also affect membrane permeability and leakage of encapsulated molecules of different sizes [48]. Membrane permeability and pores formed in the reconstructed membrane vesicle are a major advantage in the potential application of such vesicles for drug delivery, as there is considerable effort to develop self-assembling nanovesicles and artificial cells containing membranes that can be easily manipulated to transport cargo into and out of internal compartments [49]. Skinkle et al. (2020) investigated the distribution of pore size in a population of giant plasma membrane vesicles derived from rat basophilic leukemia cells [50]. They also found heterogeneity in pore size, likely due to the shear stress that occurs during vesicle formation. In particular, the vesicles were impermeable to dextrans with a molecular weight of 40 kDa and above.

The results showed that the surface properties of the reconstructed vesicles were similar to those of the mother cells in terms of rigidity and hydrophilicity (Fig. 5). The average rigidity of *D. tertiolecta* grown at a salinity of 38 corresponds to 3.5 kPa [51], while the rigidity of the reconstructed vesicles is about ten times lower due to the lack of cytoskeletal network within the vesicle. In addition, cells and vesicles

behave hydrophilically [51], which is consistent with the identified lipid classes and their ratio. The most important observed feature is that the ratio of lipid classes of the mother cell and the reconstructed membrane vesicles is not significantly perturbed (Fig. 6). All lipid classes of *D. tertiolecta* are involved in the formation of the reconstituted membrane, where they play a fundamental role in maintaining membrane structure, suggesting high utilization. Moreover, the ratio of proteins: lipids: carbohydrates per reconstructed membrane vesicle corresponds to 29.76 pg: 2.63 pg: 25.8 pg, so that the protein content predominates, which is consistent with the first study by Jokela [39]. For the first time, 47 proteins were identified and determined to be derived from the cytoplasm and chloroplasts (Fig. 7, Table S1). Although, the reconstructed membrane vesicles show weak autofluorescence (Fig. S3b) at the wavelength of chlorophyll [24], the presence of a corresponding chlorophyll *a-b* binding protein as found in the mother cells (unpublished data) was not identified here, probably due to signal suppression by other protein classes. Therefore, we will perform further protein profiling studies. On the other hand, protein analyzes have been performed for mammalian cell-derived extracellular vesicles to predict therapeutic responses of these drug carriers [52,53]. However, little is known about the protein profiles in extracellular vesicles from plants and algae under different culture conditions and how much protein is integrated into the vesicles. Indeed, extracellular vesicles from plants invaded by pathogens show enrichment of proteins involved in signal transduction in response to biotic and abiotic stresses, proteins responsible for immunity, and enzymes that remodel the cell wall [54]. In addition, cytosolic proteins, metabolic enzymes, chaperones, hydrolases, and membrane channels/transporters have been identified in various plant vesicles. Aquaporins have been reported to play an important role in vesicle stability in plasma membrane vesicles purified from broccoli plants [55]. In the reconstructed membrane vesicles of *D. tertiolecta*, we identified proteins involved in the carbohydrate metabolic process, cellular amino acid biosynthetic process, photosynthesis, oxidoreductase activity, and microtubule-based process. Although further studies are needed, we can assume that proteins involved in microtubule-based processes (tubulin alpha and beta chains) may be responsible for the stability of the reconstructed vesicles [56]. The microtubule networks were only associated with the membrane of the vesicle, as shown in Fig. S3a. Microtubulins have also been reported to be a target for anticancer drugs [57].

The reconstructed membrane vesicles differ in the transport ability of calcein, FITC-ovalbumin, and FITC-concanavalin A due to the different physicochemical properties of the dye and the structural features of the membrane (Fig. 8). Calcein is a small hydrophilic molecule (Mw = 0.6 kDa) with a hydrodynamic radius of 0.74 nm [58], which is much smaller than the determined pore size of the membrane. Therefore, calcein spontaneously permeates the vesicle membrane. FITC-ovalbumin, a globular protein (Mw = 43 kDa), does not penetrate or interact with the vesicle membrane and therefore cannot be considered a drug cargo (Fig. 8e). FITC-concanavalin A is a carbohydrate-binding protein that consists of 4 subunits and has a molecular weight of 104 kDa. When the dye was added to the immobilized vesicles, a different behavior was observed compared with calcein and ovalbumin (Fig. 8h). As the figure shows, the high fluorescence intensity of FITC-concanavalin A on the membrane itself is probably due to specific interactions with glucose and mannose units and glycoconjugates on the membrane [59]. This is confirmed by the fact that the mother cell of *D. tertiolecta* contains glycocalyx [40], and glycolipids [51] and carbohydrate content were determined. Moreover, FITC-concanavalin A also showed specific binding to the cell wall of the algal cells of *Evernia prunastri* and *Xanthoria parietina thalli* [59]. Continuing our studies to find an effective targeted delivery vehicle, we have previously reported the study of the interaction of mannosylated liposomes with concanavalin A, where the affinity of concanavalin A for mannose molecules on the surface of the liposome is increased by the presence of a multivalent ligand [60,61]. The efficiency of drug entrapment depends largely on the methods used for drug delivery, which affect the structural and functional properties of the vesicles [62]. Our previous study shows how the efficiency of entrapment depends on the nonspecific interactions between the model protein ovalbumin and phospholipids in the liposomal membrane [63].

We wondered if we could match the surface properties of the reconstructed membrane vesicles? To answer this question, the surface properties of the parent cell (alga) used for vesicle preparation must be known. For example, the surface properties of *D. tertiolecta* cells in non-axenic culture depend on the growth phase [64]. Cells of *D. tertiolecta* in the exponential growth phase are much stiffer and more hydrophobic than cells in the stationary growth phase, which are softer and more hydrophilic. We have not observed, bacterial aggregates in culture or marine bacteria adhering to the hydrophilic algal surface [65] at the nanometer scale using AFM, so they may not affect the surface properties of algal cells. The surface properties of algal cells change when exposed to abiotic stress conditions by varying temperature, salinity, and heavy metal presence [51,66,67]. The results showed that *Dunaliella* became statistically significantly stiffer at 12 °C and behaved hydrophilically over a wide range of temperatures, while *Dunaliella* behaved almost neutrally under favorable conditions (18 °C, salinity of 38). On the other hand, *Dunaliella* became statistically significantly stiffer when cells were exposed to salinity 9, where they behaved hydrophobically. Thus, by manipulating the cultivation conditions of the mother cells, the desired surface properties and thus the chemical composition of the reconstructed membrane vesicle can be achieved. For example, an increase in the relative content and unsaturation of MGDG, the major class present in both the mother cell and the reconstructed membrane vesicles, can be achieved by reducing the salinity of the *D. tertiolecta* growth medium [68]. Cultivation at temperatures above the optimum and the lack of nitrogen nutrients lead to an accumulation of lipids in the cell of *Chaetoceros pseudocurvisetus*, taking into account that growth and reproduction are slowed down under unfavorable cultivation conditions [69]. Increasing irradiance leads to the accumulation of triglycerides in the cells of *Dunaliella viridis* [70]. The accumulation of lipids, proteins, and carbohydrates in cultures of *Nannochloropsis sp*. and *Tetraselmis sp*. at pH 7.5 and 8.5 was reported in contrast to cell growth at pH 7 [71].

5. Conclusions

For the first time, reconstructed membrane vesicles from microalgae were characterized with respect to their nanomorphology, surface properties, composition, and transportability of model molecules. The microalgal cell *Dunaliella tertiolecta*, which has only a glycocalyx-like cell envelope, is a good candidate to achieve high yield in the preparation of micrometer-sized reconstructed membrane vesicles. The vesicles imaged by AFM have a rather round shape and are found in both depleted and non-depleted states. They exhibit a densely packed spherical surface structure, which could indicate surface proteins with different functions. Pits were mapped between the spherical surface structures, which could indicate pore-like structures, as large as 10 nm, as determined by permeability tests. In terms of composition, the reconstructed membrane vesicles contain about 11 times more proteins than membrane lipids. All lipid classes and their ratios in the mother cell are involved in the formation of the reconstituted membrane, where they play a fundamental role in maintaining membrane structure, suggesting high utilization.The results show that the vesicles are very soft (less than kPa), and hydrophilic, and retain the surface properties of the mother cell. The permeability of the reconstructed membrane vesicles depends on the structural features of the membrane and the physicochemical properties of the model fluorescent dye. The vesicles are permeable to calcein, impermeable to FITC-ovalbumin, and semi-permeable to FITC-concanavalin A, probably because of specific surface interactions with the glucose and mannose moieties of the membrane, which could serve as a basis for the development of drug carriers. Finally, reconstructed membrane vesicles could pave a new way as

sustainable and environmentally friendly marine bioinspired carriers that can be efficiently fabricated and could serve for studies on micro-transport of materials and membrane-related processes that contribute to advances in life sciences and biotechnology.

Declaration of Competing Interest

The authors declare that they have no known competing financial interests or personal relationships that could have appeared to influence the work reported in this paper.

Data availability

Data will be made available on request.

Acknowledgments

This work is supported by the Croatian Science Foundation projects "From algal cell surface properties to stress markers for aquatic ecosystems" (IP-2018-01-5840), "Synthesis of Supramolecular Self-assembled Nanostructures for Construction of Advanced Functional Materials" (IP-2018-01-6910), Croatia, and by the Croatian-French program "Cogito" partner Hubert Curien (Campus France n°46656ZC).

Appendix A. Supplementary material

Supplementary data to this article can be found online at https://doi.org/10.1016/j.bioelechem.2022.108360.

References

[1] A.M. Vargason, A.C. Anselmo, S. Mitragotri, The evolution of commercial drug delivery technologies, Nat. Biomed. 5 (2021) 951–967, https://doi.org/10.1038/s41551-021-00698-w.
[2] G. Pedrioli, E. Piovesana, E. Vacchi, C. Balbi, Extracellular vesicles as promising carriers in drug delivery: considerations from a cell biologist's perspective, Biology 10 (2021) 376, https://doi.org/10.3390/biology10050376.
[3] Z. Li, Y. Wang, Y. Ding, L. Repp, G.S. Kwon, Q. Hu, Cell-based delivery systems: emerging carriers for immunotherapy, Adv. Funct. Mater. 31 (2021) 2100088, https://doi.org/10.1002/adfm.202100088.
[4] I.K. Herrmann, M.J.A. Wood, G. Fuhrmann, Extracellular vesicles as a next-generation drug delivery platform, Nat. Nanotechnol. 16 (2021) 748–759, https://doi.org/10.1038/s41565-021-00931-2.
[5] L. Sercombe, T. Veerati, F. Moheimani, S.Y. Wu, A.K. Sood, S. Hua, Advances and challenges of liposome assisted drug delivery, Front. Pharmacol. 6 (2015) 286, https://doi.org/10.3389/fphar.2015.00286.
[6] A. Srivatsava, T. Yadav, S. Sharma, A. Nayak, A.A. Kumari, N. Mishra, Polymers in drug delivery, J. Biosci. Med. 4 (2016) 69–84, https://doi.org/10.4236/jbm.2016.41009.
[7] Z. Shi, Y. Zhou, T. Fan, Y. Lin, H. Zhang, L. Mei, Inorganic nano-carriers based smart drug delivery systems for tumor therapy, Smart Mater. Medic. 1 (2020) 32–47, https://doi.org/10.1016/j.smaim.2020.05.002.
[8] P. Bhatt, S. Trehan, N. Inamdar, V.K. Mourya, A. Misra, Polymers in drug delivery: an update, in: A. Misra, A. Shahiwala (Eds.), Applications of Polymers in Drug Delivery, Elsevier, 2020, https://doi.org/10.1016/B978-0-12-819659-5.00001-X.
[9] J. Delasoie, F. Zobi, Natural diatom biosilica as microshuttles in drug delivery systems, Pharmaceutics 11 (2019) 537, https://doi.org/10.3390/pharmaceutics11100537.
[10] H. Lutz, S. Hu, P.-U. Dinh, K. Cheng, Cells and cell derivatives as drug carriers for targeted delivery, Med. Drug Disc. 3 (2019), 100014, https://doi.org/10.1016/j.medidd.2020.100014.
[11] J.S. Brenner, D.C. Pan, J.W. Myerson, O.A. Marcos-Contreras, C.H. Villa, P. Patel, H. Hekierski, S. Chatterjee, J.-Q. Tao, H. Parhiz, K. Bhamidipati, T.G. Uhler, E. D. Hood, R. Yu Kiseleva, V.S. Shuvaev, T. Shuvaveva, M. Khoshnejad, I. Johnston, J.V. Gregory, J. Lahann, T. Wang, E. Cantu, W.M. Armstead, S. Mitragotri, V. Muzykantov, Red blood cell-hitchhiking boosts delivery of nanocarriers to chosen organs by orders of magnitude, Nat. Commun. 9 (2018) 2684, https://doi.org/10.1038/s41467-018-05079-7.
[12] X. Wan, S. Zhang, F. Wang, W. Fan, C. Wu, K. Mao, H. Wang, Z. Hu, Y.-G. Yang, T. Sun, Red blood cell-derived nanovesicles for safe and efficient macrophage-targeted drug deliver *in vivo*, Biomater. Sci. 7 (2019) 187–195, https://doi.org/10.1039/C8BM01258J.
[13] F. Combes, E. Meyer, N.N. Sanders, Immune cells as tumor drug delivery vehicles, J. Control. Release 327 (2020) 70–87, https://doi.org/10.1016/j.jconrel.2020.07.043.
[14] K. Kuruvinashetti, S. Pakkiriswami, M. Packirisamy, Algal extracellular vesicles for therapeutic applications, in: 2020 IEEE 20th International Conference on Nanotechnology (IEEE-NANO), 2020, pp. 354–357, doi: 10.1109/NANO47656.2020.9183452.
[15] W. Zhang, M. Wang, W. Tang, R. Wen, S. Zhou, C. Lee, H. Wang, W. Jiang, I. M. Delahunty, Z. Zhen, H. Chen, M. Chapman, Z. Wu, E.W. Howerth, H. Cai, Z. Li, J. Xie, Nanoparticle-laden macrophages for tumor-tropic drug delivery, Adv. Mater. 30 (2018) 1805557, https://doi.org/10.1002/adma.201805557.
[16] N.L. Klyachko, R. Polak, M.J. Haney, Y. Zhao, R.J. Gomes Neto, M.C. Hill, A. V. Kabanov, R.E. Cohen, M.F. Rubner, E.V. Batrakova, Macrophages with cellular backpacks for targeted drug delivery to the brain, Biomaterials 140 (2017) 79–87, https://doi.org/10.1016/j.biomaterials.2017.06.017.
[17] D. Vorselen, S.M. van Dommelen, R. Sorkin, M.C. Piontek, J. Schiller, S.T. Döpp1, S A.A. Kooijmans, B.A. van Oirschot, B.A. Versluijs, M.B. Bierings, R. van Wijk, R.M. Schiffelers, G.J.L. Wuite, W.H. Roos, The fluid membrane determines mechanics of erythrocyte extracellular vesicles and is softened in hereditary spherocytosis, Nat. Commun. 9 (2018) 4960, doi: 10.1038/s41467-018-07445-x.
[18] S. Gill, R. Catchpole, P. Forterre, Extracellular membrane vesicles in the three domains of life and beyond, FEMS Microbiol. Rev. 43 (2019) 273–303, https://doi.org/10.1093/femsre/fuy042.
[19] F. Bayat, A. Afshar, N. Baghban, Allgal cells-derived extracellular vesicles: a review with special emphasis on their microbial effects, Front. Microbiol. 12 (2021), 785716, https://doi.org/10.3389/fmicb.2021.785716.
[20] C. Tramontano, G. Chianese, M. Terracciano, L. de Stefano, I. Rea, Nanostructured biosilica of diatoms: from water world to biomedical applications, Appl. Sci. 10 (2020) 6811, https://doi.org/10.3390/app10196811.
[21] G. Adamo, D. Fierli, D.P. Romancino, S. Picciotto, M.E. Barone, A. Aranyos, D. Božič, S. Morsbach, S. Raccosta, C. Stanly, C. Paganini, M. Gai, A. Cusimano, V. Martorana, R. Noto, R. Carrotta, F. Librizzi, L. Randazzo, R. Parkes, U. C. Palmiero, E. Rao, A. Paterna, P. Santanicola, A. Iglič, L. Corcuera, A. Kisslinger, E. Di Schiavi, G.L. Liguori, K. Landfester, V. Kralj-Iglič, P. Arosio, G. Pocsfalvi, N. Touzet, M. Manno, A. Bongiovanni, Nanoalgosomes: Introducing extracellular vesicles produces by microalgae, J. Extracell. Vesicles 10 (2021) e12081.
[22] S. Picciotto, M.E. Barone, D. Fierli, A. Aranyos, G. Adamo, D. Božič, D. P. Romancino, C. Stanly, R. Parkes, S. Morsbach, S. Raccosta, C. Paganini, A. Cusimano, V. Martorana, R. Noto, R. Carrotta, F. Librizzi, U.C. Palmiero, P. Santonicola, A. Iglič, M. Gai, L. Corcuera, A. Kisslinger, E. Di Schiavi, K. Lanfester, G.L. Liguori, V. Kralj-Iglič, P. Arosio, G. Pocsfalvi, M. Manno, N. Touzet, A. Bongiovanni, Isolation of extracellular vesicles from microalgae: towards the production of sustainable and natural nanocarriers of bioactive compounds, Biomater. Sci. 9 (2021) 2917–2930, https://doi.org/10.1039/d0bm01696a.
[23] S. Jin, K. Ye, Nanoparticle-mediated drug delivery and gene therapy, Biotechnol. Prog. 23 (2007) 32–41, https://doi.org/10.1021/bp060348j.
[24] N. Ivošević DeNardis, G. Pletikapić, R. Frkanec, L. Horvat, P.T. Vernier, From algal cells to autofluorescent ghost plasma membrane vesicles, Bioelectrochemistry 134 (2020), 107524, https://doi.org/10.1016/j.bioelechem.2020.107524.
[25] R.R.L. Guillard, Culture of phytoplankton for feeding marine invertebrates, in: W. L. Smith, M.H. Chanley (Eds.), Culture of Marine Invertebrate Animals, Springer, Boston, MA, USA, 1975, pp. 29–60, https://doi.org/10.1007/978-1-4615-8714-9_3.
[26] G. Pletikapić, T. Mišić Radić, A. Hozić Zimmermann, V. Svetličić, M. Pfannkuchen, D. Marić, J. Godrijan, V. Žutić, AFM imaging of extracellular polymer release by marine diatom *Cylindrotheca closterium* (Ehrenberg) Reiman & J. C. Lewin, J. Mol. Recognit. 24 (2011) 436–445, https://doi.org/10.1002/jmr.1114.
[27] J.L. Hutter, J. Bechhoefer, Calibration of atomic-force microscope tips, Rev. Sci. Instrum. 64 (1993) 1868–1873, https://doi.org/10.1063/1.1143970.
[28] H. Hertz, Ueber die Berührung fester elastischer Körper. J. für die Reine und, Angew. Math. (1981) 156–171, https://doi.org/10.1515/crll.1882.92.156.
[29] I. Demir, I. Lüchtefeld, C. Lemen, E. Dague, P. Guiraud, T. Zambelli, C. Formosa-Dague, Probing the interactions between air bubbles and (bio)interfaces at the nanoscale using FluidFM technology, J. Colloid Interf. Sci. 604 (2021) 785–797, https://doi.org/10.1016/j.jcis.2021.07.036.
[30] E.G. Bligh, W.J. Dyer, A rapid method of total lipid extraction and purification, Can. J. Biochem. Physiol. 37 (1959) 911–917, https://doi.org/10.1139/o59-099.
[31] B. Gašparović, S.P. Kazazić, A. Cvitešić, A. Penezić, S. Frka, Improved separation and analysis of glycolipids by Iatroscan thin-layer chromatography–flame ionization detection, J. Chromatog. A 1409 (2015) 259–267, https://doi.org/10.1016/j.chroma.2015.07.047.
[32] B. Gašparović, S.P. Kazazić, A. Cvitešić, A. Penezić, S. Frka, Corrigendum to "Improved separation and analysis of glycolipids by Iatroscan thin-layer chromatography–flame ionization detection" [J Chromatogr A 1409 (2015) 259–267], J. Chromatog, A 1521 (2017) 168–169, doi: 10.1016/j.chroma.2017.09.038.
[33] N.J. Kruger, The Bradford method for protein quantitation, in: J.M. Walker (Ed.), The Protein Protocols Handbook, Humana Press Totowa, NJ, USA, 2009, pp. 17–24, https://doi.org/10.1007/978-1-59745-198-7_4.
[34] S. Dekić Rozman, A. Butorac, R. Bertoša, J. Hrenović, M. Markeš, Loss of thermotolerance in antibiotic-resistant *Acinetobacter baumannii*, Int. J. Environ. Health Res. 32 (2022) 1581–1593, https://doi.org/10.1080/09603123.2021.1898550.
[35] A. Meister, M. Gabi, P. Behr, P. Studer, J. Vörös, P. Niedermann, J. Bitterli, J. Polesel-Maris, M. Liley, H. Heinzelmann, T. Zambelli, FluidFM: combining atomic force microscopy and nanofluidics in a universal liquid delivery system for single cell applications and beyond, Nano Lett. 9 (2009) 2501–2507, https://doi.org/10.1021/nl901384x.
[36] I. Demir-Yilmaz, N. Yakovenko, C. Roux, P. Guiraud, F. Collin, C. Coudret, A. Ter Halle, C. Formosa-Dague, The role of microplastics in microalgae cells aggregation:

a study at the molecular scale using atomic force microscopy, Sci. Total Environ. 832 (2022), 155036, https://doi.org/10.1016/j.scitotenv.2022.155036.
[37] D. Alsteens, E. Dague, P.G. Rouxhet, A.R. Baulard, Y.F. Dufrêne, Direct measurement of hydrophobic forces on cell surfaces using AFM, Langmuir 23 (2007) 11977–11979, https://doi.org/10.1021/la702765c.
[38] E. Dague, D. Alsteens, J.-P. Latgé, C. Verbelen, D. Raze, A.R. Baulard, Y.F. Dufrêne, Chemical force microscopy of single live cells, Nano Lett. 7 (2007) 3026–3030, https://doi.org/10.1021/nl071476k.
[39] A. Tang Chung-Chau Jokela, Outer Membrane of Dunaliella tertiolecta: Isolation and Properties, Ph.D. Thesis, University of California, 1969.
[40] M.A. Borowitzka, L.J. Borowitzka, Dunaliella, in: M.A. Borowitzka, L.J. Borowitzka (Eds.), Micro-algal Biotechnology, Cambridge University Press, Cambridge, UK, 1988, pp. 27–58.
[41] A. Katz, P. Waridel, A. Shevchenko, U. Pick, Salt-induced changes in the plasma membrane proteome of the halotolerant alga *Dunaliella salina* as revealed by blue native gel electrophoresis and nano-LC-MS/MS analysis, Mol. Cell. Proteomics 6 (2007) 1459–1472, https://doi.org/10.1074/mcp.M700002-MCP200.
[42] A. Ben-Amotz, J.E.W. Polle, D.V. Subba Rao, The Alga Dunaliella: Biodiversity, Physiology, Genomics and Biotechnology, first ed., Enfield, NH, USA, 2009.
[43] M. Takeuchi, H. Miyamoto, Y. Sako, H. Komizu, A. Kusumi, Structure of the erythrocyte membrane skeleton as observed by atomic force microscopy, Biophys. J. 74 (1998) 2171–2183, https://doi.org/10.1016/S0006-3495(98)77926-3.
[44] A.H. Swihart, J.M. Mikrut, J.B. Ketterson, R.C. Macdonald, Atomic force microscopy of the erythrocyte membrane skeleton, J. Microsc. 204 (2001) 212–225, https://doi.org/10.1046/j.1365-2818.2001.00960.x.
[45] J.-Y. Wang, L.-P. Wang, Q.-S. Ren, Atomic force microscope observation on biomembrane before and after peroxidation, Biophys. Chem. 131 (2007) 105–110, https://doi.org/10.1016/j.bpc.2007.09.010.
[46] H. de Balmann, R. Nobrega, The deformation of dextran molecules. Causes and consequences in ultrafiltration, J. Membrane Sci. 40 (1989) 311–327, https://doi.org/10.1016/S0376-7388(00)81153-9.
[47] H. Wen, J. Hao, S.K. Li, Characterization of human sclera barrier properties for transscleral delivery of Bevacizumab and Ranibizumab, J. Pharm. Sci. 102 (2013) 892–903, https://doi.org/10.1002/jps.23387.
[48] H.P. Erickson, Size and shape of protein molecules at the nanometer level determined by sedimentation, gel filtration, and electron microscopy, Biol. Proced. Online. 11 (2009) 32, doi: 10.1007/s12575-009-9008-x.
[49] C.E. Hilburger, M.L. Jacobs, K.R. Lewis, J.A. Peruzzi, N.P. Kamat, Controlling secretion in artificial cells with a membrane AND Gate, ACS Synth. Biol. 8 (2019) 1224–1230, https://doi.org/10.1021/acssynbio.8b00435.
[50] A.D. Skinkle, K.R. Levental, I. Levental, Cell-derived plasma membrane vesicles are permeable to hydrophilic molecules, Biophys. J. 118 (2020) 1292–1300, https://doi.org/10.1016/j.bpj.2019.12.040.
[51] N. Novosel, T. Mišić Radić, M. Levak Zorinc, J. Zemla, M. Lekka, I. Vrana, B. Gašparović, L. Horvat, D. Kasum, T. Legović, P. Žutinić, M. Gligora Udovič, N. Ivošević DeNardis, Salinity induced chemical, mechanical and behavioral changes in marine microalgae, J. Appl. Phycol. 34 (2022) 1293–1309, https://doi.org/10.1007/s10811-022-02734-x.
[52] F. Tian, S. Zhang, C. Liu, Z. Han, Y. Liu, J. Deng, Y. Li, X. Wu, L. Cai, L. Qin, Q. Chen, Y. Yuan, Y. Liu, Y. Cong, B. Ding, Z. Jiang, J. Sun, Protein analysis of extracellular vesicles to monitor and predict therapeutic response in metastatic breast cancer, Nat. Commun. 12 (2021) 2536, https://doi.org/10.1038/s41467-021-22913-7.
[53] C. Charoenviriyakul, Y. Takanashi, M. Nishikawa, Y. Takakura, Preservation of exosomes at room temperature using lyophilization, Int. J. Pharmac. 553 (2018) 1–7, https://doi.org/10.1016/j.ijpharm.2018.10.032.
[54] E. Woith, G. Guerriero, J.-F. Hausman, J. Renaut, C.C. Leclercq, C. Weise, S. Legay, A. Wang, M.F. Melzig, Plant extracellular vesicles and nanovesicles: focus on secondary metabolites, proteins and lipids with perspectives on their potential and sources, Int. J. Mol. Sci. 22 (2021) 3719, https://doi.org/10.3390/ijms22073719.
[55] M. Alfieri, A. Leone, A. Ambrosone, Plant-derived nano and microvesicles for human health and therapeutic potential in nanomedicine, Pharmaceutics 13 (2021) 498, https://doi.org/10.3390/pharmaceutics13040498.
[56] G.M. Cooper, The Cell: A Molecular Approach, second ed., Sunderland, MA, USA, 2000.
[57] T. Hashimoto, Microtubules in plants, TAB 13 (2015), https://doi.org/10.1199/tab.0179.
[58] Y. Tamba, H. Ariyama, V. Levadny, M. Yamazaki, Kinetic pathway of antimicrobial peptide magainin 2-induced pore formation in lipid membranes, J. Phys. Chem. B 114 (2010) 12018–12026, https://doi.org/10.1021/jp104527y.
[59] B. Fontaniella, A.M. Millanes, C. Vincente, M.-E. Legaz, Concanavalin A binds to a mannose-containing ligand in the cell wall of some lichen phycobiants, Plant Pyhsiol. Biochem. 42 (2004) 773–779, https://doi.org/10.1016/j.plaphy.2004.09.003.
[60] A. Štimac, J. Trmčić Cvitaš, L. Frkanec, O. Vugrek, R. Frkanec, Design and syntheses of mono and multivalent mannosyl-lipoconjugates for targeted liposomal drug delivery, Int. J. Pharmaceut. 511 (2016) 44–56, https://doi.org/10.1016/j.ijpharm.2016.06.123.
[61] A. Štimac, S. Šegota, M. Dutour Sikirić, R. Ribić, L. Frkanec, V. Svetličić, S. Tomić, B. Vranešić, R. Frkanec, Surface modified liposomes by mannosylated conjugates anchored via the adamantyl moiety in the lipid bilayer, BBA-Biomembrane 1818 (2012) 2252–2259, doi: 10.1016/j.bbamem.2012.04.002.
[62] B.F. Hettich, J.J. Bader, J.C. Leroux, Encapsulation of hydrophilic compounds in small extracellular vesicles: loading capacity and impact on vesicle functions, Adv. Healthc. Mater. 11 (2022) 2100047, https://doi.org/10.1002/adhm.202100047.
[63] M. Brgles, D. Jurašin, M. Dutour Sikirić, R. Frkanec, J. Tomašić, Entrapment of ovalbumin into liposomes – factors affecting entrapment efficiency, liposome size and zeta potential, J. Liposome Res. 18 (2008) 235–248, https://doi.org/10.1080/08982100802312762.
[64] F. Pillet, E. Dague, J. Pečar Ilić, I. Ružić, M.-P. Rols, N. Ivošević DeNardis, Changes in nanomechanical properties and adhesion dynamics of algal cells during their growth, Bioelectrochemistry 128 (2019) 154–162, https://doi.org/10.1016/j.bioelechem.2019.02.011.
[65] V. Žutić, N. Ivošević, V. Svetličić, R.A. Long, F. Azam, Film formation by marine bacteria at a model fluid interface, Aquat. Microb. Ecol. 17 (1999) 231–238, https://doi.org/10.3354/ame017231.
[66] N. Novosel, T. Mišić Radić, J. Zemla, M. Lekka, A. Čačković, D. Kasum, T. Legović, P. Žutinić, M. Gligora Udovič, N. Ivošević DeNardis, Temperature-induced response in algal cell surface properties and behaviour: an experimental approach, J. Appl. Phycol. 34 (2021) 243–259, https://doi.org/10.1007/s10811-021-02591-0.
[67] N. Ivošević DeNardis, J. Pečar Ilić, I. Ružić, N. Novosel, T. Mišić Radić, A. Weber, D. Kasum, Z. Pavlinska, R.K. Balogh, B. Hajdu, Balint, A. Marček Chorvátová, B. Gyurcsik Algal cell response to laboratory-induced cadmium stress: a multimethod approach, Eur. Biophys. J. 48 (2019) 124–142, doi: 10.1007/s00249-019-01347-6.
[68] I. Vrana, S. Bakija Alempijević, N. Novosel, N. Ivošević DeNardis, D. Žigon, N. Ogrinc, B. Gašparović, Hyposalinity induces significant polar lipid remodeling in the marine microalga *Dunaliella tertiolecta* (Chlorophyceae), J. Appl. Phycol. 34 (2022) 1457–1470, https://doi.org/10.1007/s10811-022-02745-8.
[69] L. Flanjak, I. Vrana, A. Cvitešić Kušan, J. Godrijan, T. Novak, A. Penezić, B. Gašparović, Effects of high temperatures and nitrogen availability on the growth and composition of the marine diatom *Chaetoceros pseudocurvisetus*, J. Exp. Bot. 73 (2022) 4250–4265, https://doi.org/10.1093/jxb/erac145.
[70] F.J.L. Gordillo, M. Goutx, F.L. Figueroa, F.X. Niell, Effects of light intensity, CO_2 and nitrogen supply on lipid class composition of *Dunaliella viridis*, J. Appl. Phycol. 10 (1998) 135–144, https://doi.org/10.1023/A:1008067022973.
[71] H. Khatoon, N.A. Rahman, S. Banerjee, N. Harun, S.S. Suleiman, N.H. Zakaria, F. Lananan, S.H.A. Hamid, A. Endut, Effects of different salinities and pH on the growth and proximate composition of *Nannochloropsis* sp and *Tetraselmis sp* isolated from South China Sea cultured under control and natural condition, Int. Biodeter. Biodegr. 95 (2014) 11–18, https://doi.org/10.1016/j.ibiod.2014.06.022.